Cellular and Molecular Life Sciences (2025) 82:37
https://doi.org/10.1007/s00018-024-05530-7

Cellular and Molecular Life Sciences

ORIGINAL ARTICLE

Connexin 43 contributes to perioperative neurocognitive disorder by attenuating perineuronal net of hippocampus in aged mice

Qian Zhang[1] · Yuxin Zhang[1] · Peilin Cong[1] · Qianqian Wu[1] · Hanxi Wan[1] · Xinwei Huang[1] · Xinyang Li[1] · Zhouxiang Li[1] · Jingxuan Li[1] · Huanghui Wu[1] · Li Tian[1] · Lize Xiong[1]

Received: 21 August 2024 / Revised: 12 November 2024 / Accepted: 24 November 2024

Abstract

Background Perioperative neurocognitive disorder (PND) is a prevalent form of cognitive impairment in elderly patients following anesthesia and surgery. The underlying mechanisms of PND are closely related to perineuronal nets (PNNs). PNNs, which are complexes of extracellular matrix primarily surrounding neurons in the hippocampus, play a critical role in neurocognitive function. Connexin 43 (Cx43) contributes to cognitive function by modulating the components of PNNs. This study was designed to investigate the specific regulatory mechanisms of Cx43 on PNNs and its pivotal role in the development of PND.

Methods Eighteen-month-old wild-type and *Gja1*$^{fl/fl}$ C57BL/6 mice were subjected to abdominal surgery under 1.4% isoflurane anesthesia. Cognitive functions, particularly learning and memory, were evaluated via the Y-maze test, Barnes maze (BM) and contextual fear conditioning test (CFT). The mRNA and protein expression levels of Cx43 were assessed by using quantitative reverse transcription polymerase chain reaction (qRT-PCR), fluorescent in situ hybridization (FISH), western blotting and flow cytometry. The quantity of PNNs was measured by *Wisteria floribunda* agglutinin (WFA) and Aggrecan staining.

Results Aged mice subjected to anesthesia and surgery exhibited deficits in hippocampus-dependent cognitive functions, which were accompanied by increased Cx43 mRNA and protein expression. Conditional knockout (cKO) of Cx43 in astrocytes alleviated cognitive deficits and promoted the number of PNNs and dendritic spines in the hippocampus by targeting Dmp1. Knockdown of *Dmp1* attenuated the beneficial effects of Cx43 cKO on cognitive deficits induced by anesthesia and surgery.

Conclusion Our findings indicate that anesthesia and surgery induce an increase in Cx43 expression, which inhibits the formation of PNNs and dendritic spines in hippocampus by suppressing *Dmp1* transcription, leading to cognitive deficits in aged mice. These results offer new mechanistic insights into the pathogenesis of PND and identify potential targets for therapeutic intervention.

Keywords Connexin 43 · Perioperative neurocognitive disorder · Perineuronal nets

Qian Zhang, Yuxin Zhang and Peilin Cong contributed equally.

✉ Huanghui Wu
mzkwhh@126.com

✉ Li Tian
13992868902@163.com; ltian@tongji.edu.cn

✉ Lize Xiong
mzkxlz@126.com; lizexiong@tongji.edu.cn

[1] Shanghai Key Laboratory of Anesthesiology and Brain Functional Modulation, Clinical Research Center for Anesthesiology and Perioperative Medicine, Translational Research Institute of Brain and Brain-Like Intelligence, Department of Anesthesiology and Perioperative MedicineSchool of Medicine, Shanghai Fourth People's Hospital, School of Medicine, Tongji University, 1239 Sanmen Road, Hongkou District, Shanghai 200434, China

Published online: 06 January 2025

Introduction

Perioperative neurocognitive disorder (PND) is a syndrome characterized by a decline in cognitive performance across a range of neuropsychological tests, including assessments of working memory, long-term memory, and mental flexibility, particularly during the perioperative period and predominantly in elderly patients [1–5]. The incidence of PND fluctuates based on perioperative and intraoperative risk factors, with reported rates as high as 53.3% [6]. PND can persist for several months, significantly reduce the quality of life for affected patients and consequently imposing substantial social and economic burdens [7–9]. Regrettably, effective interventions for PND are still scarce. Therefore, a deeper comprehension of the pathophysiological mechanisms underpinning PND is essential. Research has indicated that cognitive dysfunction is often linked to alterations in the extracellular matrix [10, 11]. However, due to the paucity of studies, the specific mechanisms by which the extracellular matrix is implicated in cognitive decline following anesthesia and surgery in aged mice remain unclear.

Prior preclinical and clinical studies have demonstrated that injury to the extracellular matrix occurs following anesthesia and surgery, which can ultimately impair brain function [12–14]. Perineuronal nets (PNNs) represent the most prominent structures of the extracellular matrix, predominantly encircling the soma and dendrites of specific neurons across various brain regions. They are composed of a proteoglycan core protein adorned with chondroitin sulfate chains [15, 16]. Functionally, PNNs are involved in the stabilization of synapses by serving as a physical barrier and participate in the integration and consolidation of memory by providing a continuous microenvironment that facilitates the flow of cations across the neuronal membrane [17–19]. It is noteworthy that the loss or fragmentation of PNNs has been observed following cardiac surgery [20]. Consequently, the loss of PNNs may significantly contribute to the development of PND.

Connexin 43 (Cx43), found both in the membrane and in the cytoplasm, is closely associated with neurocognitive function [21–24]. Recent groundbreaking studies have indicated that cytoplasmic Cx43 plays an active role in controlling gene expression through direct interactions with certain transcription factors [25]. In the brains of Alzheimer's disease (AD) patients and APP/PS1 mice, astroglial Cx43 immunoreactivity is significantly increased in amyloid-beta (Aβ) plaques [26]. Specific deletion of Cx43 in astrocytes has been shown to improve cognitive function in mouse models by reducing astrogliosis and enhancing synaptic function [27]. Furthermore, Cx43 deficiency was shown to enhances the expression of extracellular matrix remodeling factors [28]. However, the specific involvement of Cx43 in PNNs has not been extensively studied, and this area warrants further investigation.

This study aimed to elucidate the specific regulatory mechanisms of Cx43 on PNNs and its critical role in the development of PND. We performed anesthesia and surgery on eighteen-month-old wild-type and *Gja1*$^{fl/fl}$ C57BL/6 mice. The presence of PNNs was quantified using *Wisteria floribunda* agglutinin (WFA) and Aggrecan staining. Here, our findings indicate that the expression of Cx43 was upregulated in aged mice subsequent to anesthesia and surgery. Targeted suppression of Cx43 in astrocytes was found to be sufficient to mitigate cognitive decline before anesthesia and surgery in aged mice. We discovered that cytoplasmic Cx43 in astrocytes impeded the formation of PNNs by interacting with the transcriptional regulator Sox2 to the downregulation of the expression of dentin matrix protein1 (Dmp1).

Methods

Animal care and use

In strict adherence to the guidelines set forth by the National Research Council's "Guide for the Care and Use of Laboratory Animals," we conducted all animal procedures. The experimental protocols were granted approval by Tongji University's Animal Care and Use Committee in Shanghai, China, under the designated approval number: TJBH07922101. Random assignment of animals to experimental groups was practiced. Housing conditions for the animals included groups of 4 to 5 per cage in a controlled environment within a colony room. The temperature was consistently maintained between 19 °C and 22 °C, with humidity levels ranging from 40 to 60%. A 12-h light/dark cycle was implemented, with lighting on from 07:00 to 19:00. Animals were provided with food and water without restriction. Following a two-week period of environmental acclimation, experiments were initiated. Eighteen-month-old male C57BL/6 J mice were procured from Beijing Vital River Laboratory Animal Technology. *Gja1*$^{fl/fl}$ mice, identified by the stock number CKOAIP221129RT9, were sourced from Cyagen Biosciences, Inc., and were housed at the Shanghai Key Laboratory of Anesthesiology and Brain Functional Modulation facilities. A C57BL/6J genetic background was maintained for all transgenic mice.

PND modeling

A model of PND was established via experimental laparotomy, as detailed in a previous study [29]. Mice were initially anesthetized using 2% isoflurane in 100% oxygen at a flow rate of 1 L/min. Once the absence of the reversal

reflex was confirmed, anesthesia was sustained with 1.5% isoflurane in 100% oxygen at an equivalent flow rate. The surgical site's fur was meticulously removed, and the area was disinfected with povidone-iodine. A 2 cm longitudinal incision along the abdominal midline was made, followed by the blunt dissection of the muscle layer in the surgical group. A segment of the ileum, 3–5 cm in length and vascularized by collaterals from the same mesenteric artery, was carefully exteriorized and placed on sterile gauze moistened with normal saline. This ileum segment was gently manipulated for 10 min before being returned to the peritoneal cavity. The incision was closed using a sterile 4–0 chromic gut suture (Vicryl; Ethicon, USA). The abdominal muscles were sutured, and lidocaine ointment was applied to the incision site for analgesia post-operation. Mice in the normal control group, not subjected to laparotomy, were exempt from anesthesia and surgery.

Assessment of neurocognitive function

Behavioral evaluations took place within a soundproof environment, adhering to standard conditions. In our study, all mice, including those in control groups, underwent a battery of behavioral tests, as detailed previously with some minor adjustments [30]. The measurements were conducted in a blinded manner, occurring during the daytime of the light cycle, typically starting at 9 AM. To prevent any confounding influences, each mouse was subjected to only one behavioral test daily. A video tracking system, SMART v3.0 by Panlab and Harvard Apparatus, was employed to monitor and analyze the test outcomes. The detail description for each behavioral test were provided in Supplemental Materials.

Quantitative reverse-transcription PCR (qRT–PCR)

Our qRT-PCR procedure closely followed the detailed methods outlined in our earlier publication [30]. Utilized in this process were specific primers:

for *Gja1,* the sequences were 5′-ACAGCGGTTGAGTCAGCTTG-3′ and 5′-GAGAGATGGGGAAGGACTTGT-3′;

for *Gapdh*, serving as a control, the sequences were 5′-TGTAGACCATGTAGTTGAGGTCA-3′ and 5′- AGGTCGGTGTGAACGGATTTG-3′.

Then, qRT–PCR reactions were carried out on a Quant Studio 1 Real Time PCR system from Thermo Fisher, USA. The relative expression levels of the genes under investigation were determined using the $2^{-\Delta\Delta Ct}$ method.

Western Blotting

The technique of Western blotting was executed with a similar attention to detail as previously described [31]. The primary antibodies that were deployed included anti-Cx43 (1:1000, 26980-1-AP, Proteintech, China), anti-Aggrecan (1:1000, AB1031, Millipore, USA), anti-Dmp1 (1:1000, sc73633, Santa Cruz Biotechnology, USA), and anti-α-Tubulin (1:5000, ab18251, Abcam, USA).

Flow cytometric analysis of the mouse Hippocampus

Flow cytometry served to evaluate the expression of Cx43 in both endothelial cells and astrocytes, as well as the localization of astroglial Cx43 within the hippocampus. The hippocampal tissues were first isolated and subjected to digestion with 0.25% trypsin–EDTA (Cat# 25200056; Gibco, USA) for 10 min at 37 °C. The digestion process was halted by adding DMEM/F12 (Cat# C11330500BT; Gibco, USA) supplemented with 10% fetal bovine serum (FBS; Cat#04-001-1ACS; Biological Industries, Israel). The tissue was then pushed through a 200 μm nylon mesh, followed by centrifugation at 1500 rpm for 5 min. The pellet was resuspended in PBS with 0.5% FBS and prepared for analysis by fixing and permeabilizing with a standard kit (Cat# 554714; BD Pharmingen, USA). The samples were incubated with a set of antibodies diluted in PBS with 0.5% FBS for 30 min in a cold environment. The antibodies used for this analysis were anti-Cx43 (1:400, Cat# 26980-1-AP; Proteintech, China), anti-ACSA2-APC-Vio770 (1:50; Cat# 130-116-247; Miltenyi Biotec, Germany), anti-CD31 (1:400, Cat# 553,373; BD Pharmingen, USA), and Alexa Fluor 488-conjugated donkey anti-rabbit IgG (1:1000, Cat# 103–545-155; Jackson ImmunoResearch Laboratories). The data obtained from flow cytometry were processed using FlowJo™ v10 software (BD bioscience, USA).

In situ hybridization

Deep anesthesia was induced in the mice using isoflurane, followed by perfusion with 0.9% saline and subsequently with 4% paraformaldehyde (PFA). The brains of the mice were then extracted and subjected to postfixation in 4% PFA overnight at 4 °C. After the tissues were dehydrated in a 30% sucrose solution, they were embedded in optimal cutting temperature (OCT) compound and sectioned into 14 mm slices. The RNA in situ hybridization was performed using a PinpoRNA™ multiplex fluorescent kit (GD Pinpoease Biotech, Cat# PIF1000) in accordance with the manufacturer's protocol, with probes designed to target mouse Gja1 (Cat# 146,091-B1). After the RNAscope procedure was completed, double immunofluorescence staining was carried out as detailed in the following section.

Immunofluorescence staining technique

Our immunofluorescence staining procedure closely adhered to the detailed methods we previously reported [29]. The primary antibodies and associated reagents selected for this process included a chicken polyclonal anti-GFAP (1:500, ab254083, Abcam, UK), anti-Aggrecan (1:1000, AB1031, Millipore, USA), and *Wisteria floribunda* agglutinin (WFA) (1:100, L1516, Sigma, USA). Tissue sections were thoroughly rinsed in Tris-buffered saline containing 0.1% Triton-X 100 (TBST), followed by an incubation period with secondary antibodies: an Alexa Fluor 488-conjugated donkey anti-chicken IgG antibody (1:1000, 103–545-155, Jackson ImmunoResearch Laboratories), an Alexa Fluor 594-conjugated donkey anti-rabbit IgG antibody (1:1000, 711-585-152, Jackson ImmunoResearch Laboratories), or Oregon Green-488 conjugated NeutrAvidin biotin-binding protein (1:1000, A6374, Thermo Fisher, USA) This incubation lasted for one hour at room temperature in a light-protected environment. Nuclear staining was achieved using DAPI (62248, Thermo Fisher, USA). Fluorescence imaging was conducted with a confocal laser scanning microscope (FV3000, Olympus, Japan), capturing 2–3 fields from the hippocampal region across six consecutive sections per mouse. The intensity of fluorescence within these fields was quantified utilizing ImageJ software (NIH, USA).

Fractions of the hippocampus tissue

In the quest to prepare the 1% Triton X-100-soluble and insoluble fractions from the hippocampus, tissues of equal mass were homogenized in RIPA lysis buffer containing 1% Triton X-100 (P0013B, Beyotime) and supplemented with proteinase and phosphatase inhibitors. Post a 30-min lysis period at 4 °C, the mixture was subjected to centrifugation at 12,000 rpm for 30 min, yielding a supernatant enriched with soluble proteins, namely the non-GJ Cx43 fraction. The pellet, containing the insoluble proteins, was resuspended in RIPA buffer with the addition of 4 M urea (Cat# 57-13-6; Sigma−Aldrich, USA). After sonication, the resuspended mixture was incubated at ambient temperature for 30 min. Following this incubation, centrifugation at 12,000 rpm for 30 min at 4 °C was performed, and the resulting supernatant, containing the GJ Cx43 fraction, was collected.

In vivo stereotactic viral injections

Aged mice, eighteen months of age, underwent anesthesia using isoflurane, initiated at 2% for the induction phase and reduced to 1.4% for maintenance. This procedure facilitated the precise stereotactic injection of viral vectors into the hippocampal region (AP: −2.1 mm, ML: ± 1.6 mm, DV: −1.8 mm). A total of 400 nl of the viral suspension was delivered at a controlled rate of 100 nl per minute. The specific hippocampal targets are illustrated in Figs. 3B and 6B. Post-injection, the needle remained stationary for an additional 10 min to ensure thorough diffusion of the viral agent prior to its careful withdrawal.

For selective knockdown of astroglial Cx43 in the hippocampus of aged C57BL/6J mice, adeno-associated virus (AAV)-GfaABC1D-shRNA *Gja1* (Brain VTA) was microinjected into the bilateral hippocampus. (AAV)-NC-mCherry (Brain VTA) was microinjected as the control.

For selective knockout of astroglial Cx43 in the hippocampus of aged $Gja1^{fl/fl}$ mice, AAV-GfaABC1D-Cre (Brain VTA) was microinjected into the bilateral hippocampus. AAV-NC (Brain VTA) was injected as a control.

For selective overexpression of astroglial Cx43 in the hippocampus, AAV-DIO-*Gja1*(OE)−3 × Flag (Brain VTA) were microinjected in the bilateral hippocampus. AAV-NC (Brain VTA) was injected as a control.

For selective knockdown of astroglial Dmp1 in the hippocampus of aged $Gja1^{fl/fl}$ mice, AAV-GfaABC1D-Cre and AAV-GfaABC1D-*Dmp1*shRNA (Brain VTA) were microinjected into the bilateral hippocampus. AAV-GfaABC1D-Cre and AAV-NC (Brain VTA) was injected as a control.

Behavioral and molecular biology assessments were conducted no earlier than three weeks following viral injection, with the efficacy of the viral infection confirmed at the study's conclusion.

Generation of $Gja1^{fl/fl}$ mice and *Gja1* conditional knockout (cKO) mice

The generation of $Gja1^{fl/fl}$ mice was carried out at Tongji University, where LoxP sites were strategically inserted to flank the second exon of the *Gja1* gene within the mouse genome. Standard genotyping utilized two primers designed to flank the loxP1 site, with sequences (5′-TTCAGAGTA AAACTGGTCTAGCCT-3′ (*Gja1* F) and 5′-GTCTGTATG CCTCTAAGCAAAACG-3′ (*Gja1* R)). The presence of the wild-type allele resulted in a 136 bp band, and the modified allele with the loxP site produced a 216 bp band, as depicted in Supplemental Fig. 1A and 1B.

RNA sequencing (RNA-seq)

Employing a RNeasy Mini Kit from Qiagen, total RNA was meticulously extracted. Subsequent library construction was followed by sequencing utilizing the Illumina NovaSeq 6000 platform. CASAVA software was then applied to evaluate the quality of the obtained sequencing data. Thereafter, clean reads were aligned to the mouse genome reference (GRCm38/mm10) using HISAT2 software, version 2.0.5. The tool FeatureCounts, in its version 1.5.0-p3, was engaged to tally the reads mapped to each gene, facilitating

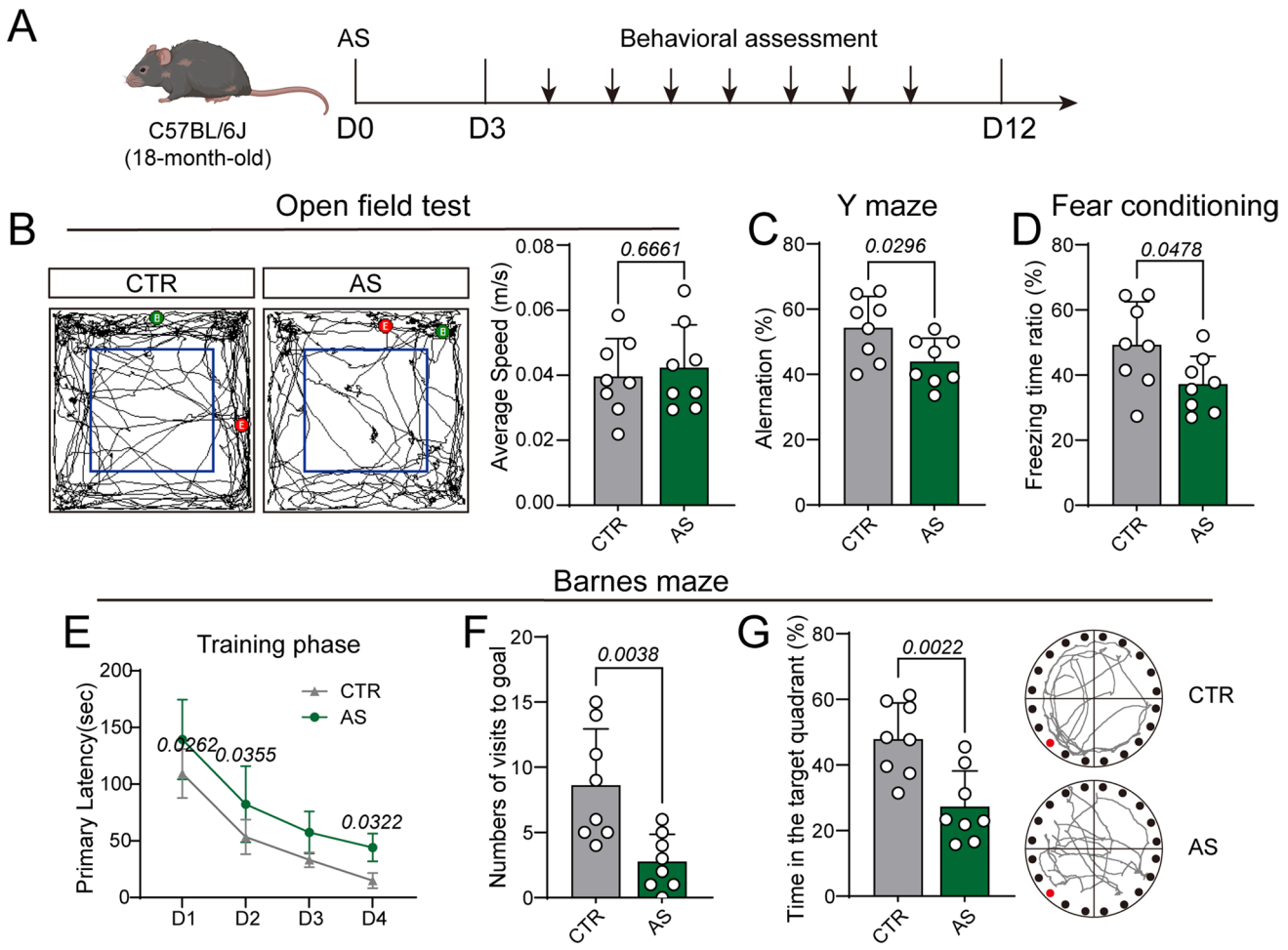

Fig. 1 Anesthesia and surgery induce cognitive decline in eighteen-month-old mice. **A** Schematic of the experimental timeline. **B** Representative trajectories and average speed in the OFT. **C** Percentage of spontaneous alternations in the Y-maze test. **D** Freezing time ratio in the CFT. **E–G** Training curve (4 consecutive days) (**E**), number of visits to the goal (**F**), time spent in the target quadrant and representative trajectories of the animals (**G**) in the BM test. The data are presented as the means ± SDs ($n = 8$ for per group), and were analyzed by two-way ANOVA or Student's *t* test. *CTR* control, *AS* anesthesia and surgery

the computation of the FPKM values. Differentiation of expressed genes was executed through DEGseq software, version 1.34.0, identifying genes with a fold change exceeding 1.5 and a false discovery rate below 0.05 as differentially expressed genes (DEGs).

Golgi staining

Morphological changes were scrutinized through the application of a Golgi-Cox staining kit (G1069, Servicebio, China). Mouse brain tissues were submerged in the Golgi solution for a duration of 14 days within a dark chamber. The tissue samples were then sectioned into 100 µm slices using a rotary microtome, transferred onto gelatin slides, and left to dry in darkness overnight. The final step involved capturing comprehensive images of the brain tissues with the aid of a digital slice scanner.

Coimmunoprecipitation

Aged C57BL/6 mouse hippocampal tissues were harvested and immersed in a lysis buffer containing 50 mM Tris–HCl, 150 mM NaCl, 1% Lubrol, 5 mM EDTA, and a cocktail of protease inhibitors for 30 min at 4 °C. Post-centrifugation at 13,680 × g for 30 min at 4 °C, the supernatants were collected. These were further incubated with specific antibodies and protein A/G Sepharose beads from Santa Cruz Biotechnology Inc., overnight at 4 °C. The complexes of antibody/antigen/Sepharose beads were washed four times using a wash buffer consisting of 10 mM Tris–HCl, 150 mM NaCl, 1 mM EDTA, 1 mM EGTA, 150 mM Triton X-100, 0.2 mM sodium orthovanadate, and a mixture of protease inhibitors. The proteins were subsequently eluted and resolved by SDS-PAGE, followed by immunoblotting.

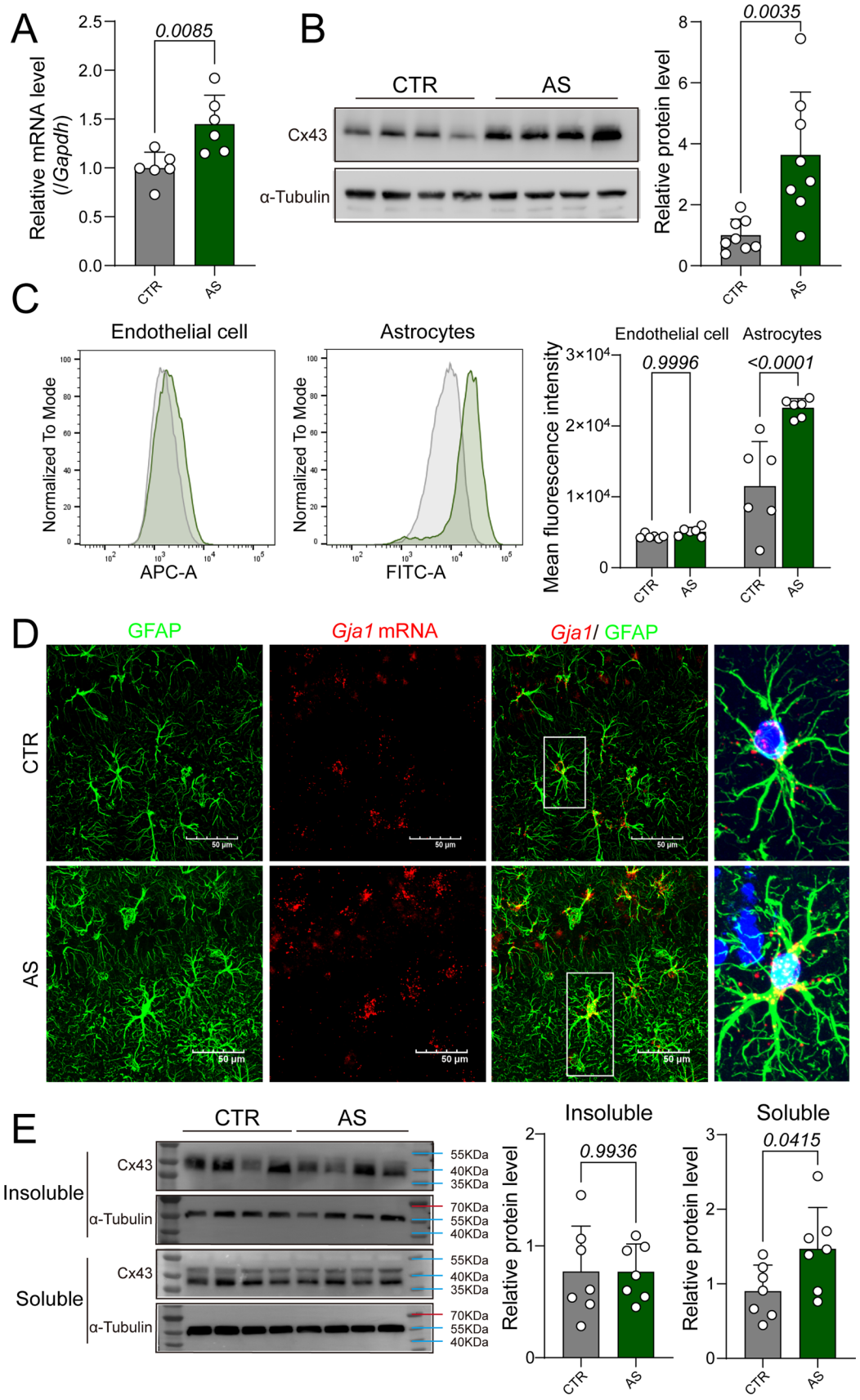
A
Relative mRNA level (/Gapdh)
0.0085
CTR
AS
B
CTR
AS
Cx43
α-Tubulin
Relative protein level
0.0035
C
Endothelial cell
Astrocytes
Normalized To Mode
APC-A
FITC-A
Mean fluorescence intensity
0.9996
<0.0001
D
GFAP
Gja1 mRNA
Gja1/ GFAP
50 μm
E
Insoluble
Soluble
55KDa
40KDa
35KDa
70KDa
0.9936
0.0415

◂**Fig. 2** Cx43 is upregulated in the hippocampus of aged mice after anesthesia and surgery. **A** The levels of *Gja1* mRNA in the hippocampus were analyzed via quantitative RT−PCR. *Gapdh* was used for normalization. $n = 6$ for per group. **B** The protein expression of Cx43 in the hippocampus was analyzed by western blotting. α-Tubulin was used as a loading control. $n = 8$ for per group. **C** Representative flow cytometry image showing the mean fluorescence intensity of Cx43 in endothelial cells and astrocytes in the CTR and AS groups. $n = 6$ for per group. **D** Representative confocal images of *Gja1* mRNA in astrocytes (labeled with GFAP) in the hippocampus according to fluorescence in situ hybridization. $n = 6$ for per group. **E** Soluble and insoluble Cx43 levels in the hippocampus were analyzed. α-Tubulin was used as a loading control. $n = 7$ for per group. The data are presented as the means ± SDs, and were analyzed by Student's *t* test. *CTR* control, *AS* anesthesia and surgery

Statistical analysis

Data are presented as mean values ± standard deviations. The sample size and the specific statistical tests applied to each experiment are detailed within the figures and their corresponding legends. Individual animals correspond to each data point for behavioral, flow cytometry, and biochemical data. Unless specified in the figure legends, behavioral and biochemical data were analyzed using two-way or one-way ANOVA, followed by post hoc multiple comparison tests, either Bonferroni's or Tukey's, as appropriate. Significance is denoted by P values indicated in the figures and legends, with a threshold of $p < 0.05$. Statistical analysis was conducted using Prism GraphPad 9.0 software. It is important to note that all experiments and data analyses were conducted by researchers who were not aware of the genotype or treatment of the samples, ensuring a blinded approach.

Results

Anesthesia and surgery lead to cognitive deficits in eighteen-month-old mice, coincident with the upregulation of Cx43 expression in the hippocampus

To elucidate the role of Cx43 in PND, we initially assessed behavioral changes and Cx43 expression levels in aged mice following anesthesia and surgery. As depicted in Fig. 1B, the average speed of mice in the control group (CTR) during the OFT was comparable to that of the anesthesia and surgery group (AS). However, a significant reduction in the percentage of spontaneous alternations was observed in the Y-maze test for the AS group relative to the CTR group (Fig. 1C). Mice that underwent anesthesia and surgery exhibited a diminished freezing time ratio in the CFT (Fig. 1D). Furthermore, in the BM test, an increase in latency during the training phase was noted (Fig. 1E), along with a decrease in the number of visits to the goal (Fig. 1F), and a reduction in the time spent in the target quadrant during the probe phase (Fig. 1G). Collectively, these findings indicate that anesthesia and surgery can lead to significant cognitive deficits in aged mice.

Subsequently, we explored the potential involvement of Cx43 in the cognitive decline associated with anesthesia and surgery in aged mice. Our initial examination focused on quantifying the levels of *Gja1* mRNA and protein within the hippocampus region. The findings demonstrated a significant upregulation of *Gja1* levels following anesthesia and surgery (Fig. 2A). Further analysis using flow cytometry indicated that these procedures led to an increase in Cx43 levels specifically in astrocytes, with no significant changes observed in endothelial cells (Fig. 2C). RNAscope in situ hybridization, coupled with double staining, confirmed elevated *Gja1* mRNA levels expression in hippocampal GFAP-positive astrocytes of mice that had undergone anesthesia and surgery (Fig. 2D). Cx43, known to exist in two distinct conformations, showed a significant increase in both total protein levels and the soluble form after the surgical intervention in aged mice (Fig. 2B, and 2E). In aggregate, these data suggest that Cx43 expression in astrocytes is upregulated in the hippocampus of aged mice subsequent to anesthesia and surgery.

Astroglial Cx43 cKO before anesthesia and surgery alleviates neurocognitive decline in aged mice

Given our observation of the upregulation of Cx43 in conjunction with cognitive deficits in aged mice following anesthesia and surgery, we proceeded to identify the role of Cx43 in the pathogenesis of PND. To this end, we employed two distinct strategies to modulate astroglial Cx43 expression prior to the administration of anesthesia and surgery procedures in aged mice.

Initially, we employed a stereotactic approach to inject adeno-associated virus (AAV) harboring the GfaABC1D promoter driving shRNA targeted against *Gja1* (AAV-GfaABC1D-sh*Gja1*) bilaterally into the hippocampus of 18-month-old wild-type mice (Fig. 3A and B) This strategy was designed to specifically attenuate Cx43 expression in astrocytes, as evidenced by western blotting in Fig. 3C. Mice subjected to Cx43 knockdown displayed enhanced cognitive performance, characterized by an increased percentage of spontaneous alternations in the Y-maze test (Fig. 3E), reduced latency during the training phase, elevated time spent in the target quadrant during the probe phase, and augmented number of visits to the goal in the BM test (Fig. 3F–H). Furthermore, in the CFT, these mice exhibited an elevated freezing time ratio, with no discernible difference in locomotor activity (Fig. 3I). Collectively, these outcomes underscore the potential of Cx43 knockdown to ameliorate cognitive decline post anesthesia and surgery.

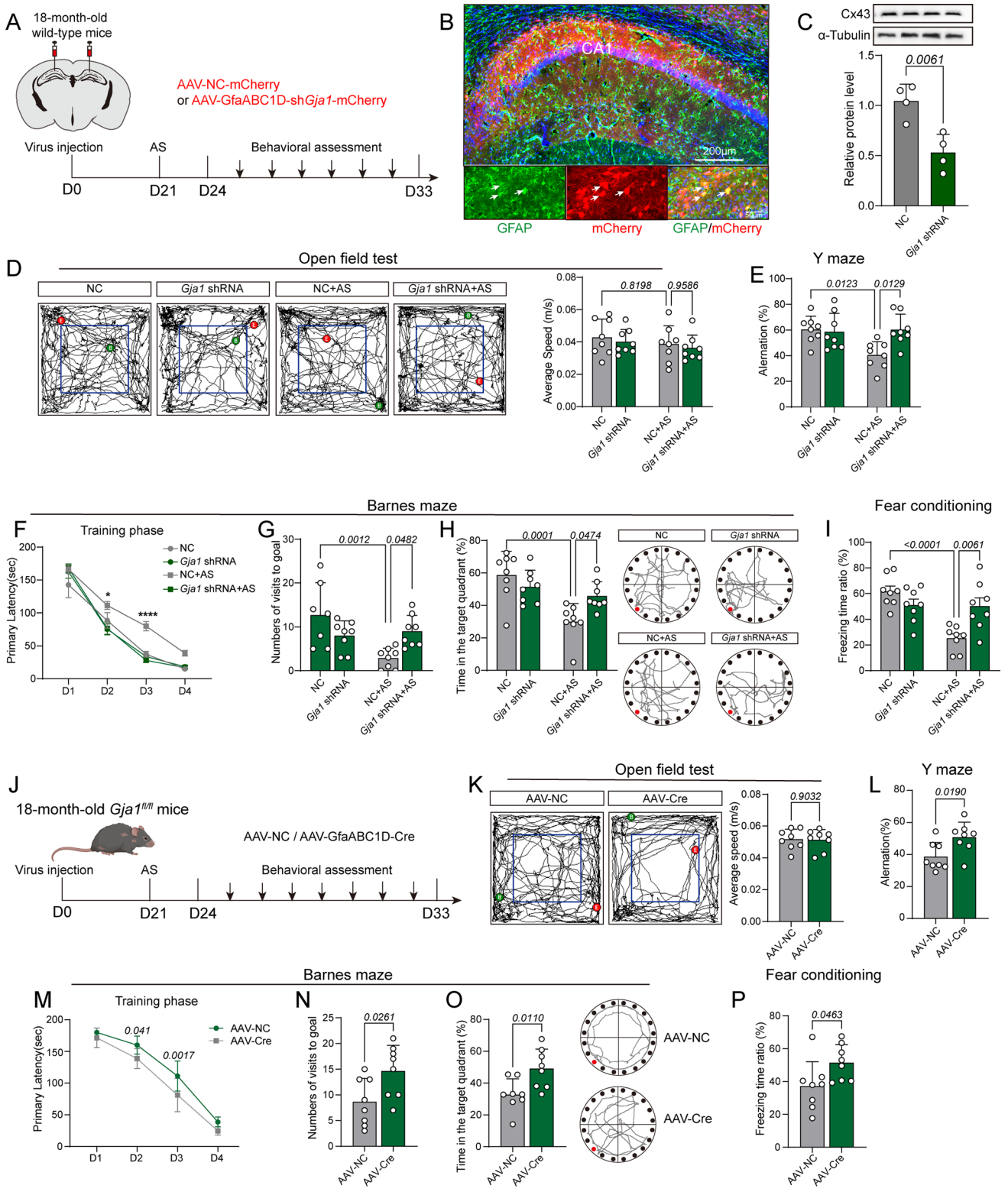

Subsequently, we generated *Gja1*-floxed mice (*Gja1*$^{fl/fl}$, Supplemental Fig. 1) to facilitate conditional knockout of Cx43. We performed stereotactic injections of AAV expressing the Cre recombinase under the control of the GfaABC1D promoter (AAV-GfaABC1D-Cre) into the bilateral hippocampus of eighteen-month-old *Gja1*$^{fl/fl}$ mice (Fig. 3J). These injections resulted in the specific deletion of Cx43 in astrocytes, which rescued the cognitive decline induced by

◂**Fig. 3** Astroglial Cx43 cKO in the hippocampus before anesthesia and surgery alleviates neurocognitive deficits in aged mice. **A** Schematic of virus injections into the bilateral hippocampus of aged mice to induce selective deletion of Cx43 in hippocampal astrocytes (top). Schematic of the experimental timeline (bottom). **B** Representative confocal images of the mouse hippocampus showing AAV-infected astrocytes in the CA1 region. Blue: DAPI staining. Scale bars, 200 μm (top). Higher magnification images showing infected CA1 astrocytes. Scale bars, 50 μm (bottom). **C** Validation of the AAV-mediated blockade of Cx43 in the hippocampus via western blotting. α-Tubulin was used as a loading control. **D** Representative trajectories and average speed in the OFT. (E) Percentage of spontaneous alternations in the Y maze test. **F–H** Training curve (4 consecutive days) (**F**), number of visits to the goal (**G**), time spent in the target quadrant and representative trajectories of the animals (**H**) in the BM test. D2: NC + AS vs. *Gja1* shRNA + AS, $*p < 0.05$; D3: NC + AS vs. *Gja1* shRNA + AS, $****p < 0.0001$. **I** Freezing time ratio in the CFT. **J** Schematic of virus injections into the bilateral hippocampus of aged $Gja1^{fl/fl}$ mice injected with AAV-NC (AAV-NC) or AAV-GfaABC1D-Cre (AAV-Cre, astroglial Cx43 cKO) into the hippocampus (top). Schematic of the experimental timeline (bottom). **K** Representative trajectories and average speed in the OFT. **L** Percentage of spontaneous alternations in the Y-maze test. **M–O** Training curve (4 consecutive days) (**M**), number of visits to the goal (**N**), time spent in the target quadrant and representative trajectories of the animals (**O**) in the BM test. **P** Freezing time ratio in the CFT. The data are presented as the means ± SDs $n = 6$ for per group. and were analyzed by one-way ANOVA, two-way ANOVA or Student's *t* test. *AS* anesthesia and surgery

anesthesia and surgery. The ameliorative effects were evident in the form of improved performance in the Y-maze probe test, as well as enhanced outcomes in the BM and CFT, without any detectable influence on locomotor activity (Fig. 3K−P). Furthermore, to explore the effects of Cx43 overexpression, we performed stereotactic injections of AAV carrying the *Gja1* gene under the GfaABC1D promoter (AAV-GfaABC1D-*Gja1*, referred to as OE) into the bilateral hippocampus of aged wild-type mice (Supplemental Fig. 2A). However, no significant behavioral changes were observed in the OFT, Y-maze, BM, or CFT (Supplemental Fig. 2B–E). In aggregate, these findings suggested that the suppression of astroglial Cx43 expression is neuroprotective against cognitive deficits induced by anesthesia and surgery.

Astroglial Cx43 cKO increases PNNs and the number of dendritic spines in hippocampal neurons

To elucidate the underlying mechanisms by which astrocyte-specific Cx43 cKO confers protection against PND, we conducted RNA sequencing (RNA-seq) on hippocampus tissue harvested from aged $Gja1^{fl/fl}$ mice that had been injected with either a control AAV (AAV-NC) or an AAV expressing Cre recombinase under the GfaABC1D promoter (AAV-Cre; Fig. 4A). The RNA-seq analysis revealed a significant upregulation of seven genes related to extracellular matrix formation in the AAV-GfaABC1D-Cre-injected mice compared to those injected with AAV-NC (Fig. 4B). The extracellular matrix is recognized for its role in neurocognitive function, yet the mechanisms underpinning this association remain not fully explored.

Further investigation was conducted to ascertain whether perineuronal nets (PNNs), known to be implicated in learning and memory deficits associated with astroglial Cx43, are affected by anesthesia and surgery. To this end, we stereotactically injected AAV-GfaABC1D-Cre (AAV-Cre) or AAV-NC (AAV-NC) into the bilateral hippocampus of aged $Gja1^{fl/fl}$ mice prior to anesthesia and surgery. PNNs were identified using WFA, which selectively binds to the glycosaminoglycan sugar side chains of PNNs glycoproteins, and visualized by labeling their core protein, Aggrecan. Our findings indicated that anesthesia and surgery led to an abolition of PNNs, and importantly, the astrocyte-specific Cx43 cKO was able to rescue this reduction in the number of PNNs in the hippocampus (Fig. 5A and B). Given the established importance of PNNs in synaptic plasticity within the central nervous system [32], we employed Golgi staining to evaluate synaptic function. In line with our previous study, a significant decrease in the number of dendritic spines was observed following anesthesia and surgery compared to the control group (AAV-NC vs. AAV-NC + AS), and this reduction was attenuated by the astrocyte-specific Cx43 cKO (Fig. 5C). Collectively, these results imply that the astrocyte-specific Cx43 cKO may enhance learning and memory in aged $Gja1^{fl/fl}$ mice by increasing the presence of PNNs and the density of dendritic spines on hippocampal neurons.

Astroglial Cx43 modulates the number of PNNs and dendritic spine in the hippocampus through Dmp1 in aged mice

To delineate the mechanisms by which Cx43 modulates PNNs and dendritic spine density in hippocampal neurons, we examined the expression changes of differentially expressed genes (DEGs) identified by RNA sequencing following anesthesia and surgery. A significant downregulation of *Dmp1* mRNA and protein levels was observed in aged wild-type mice post anesthesia and surgery (Fig. 5D and E). Our data suggest that astroglial Dmp1 may participate in Cx43-mediated PNNs formation. Dmp1, an extracellular matrix phosphoprotein and a small integrin-binding ligand, is integral to collagen formation in bone [33]. Its role in promoting extracellular matrix formation in the central nervous system (CNS) has been indicated but requires further study.

To explore the role of Dmp1 in Cx43-mediated PNNs formation, we performed stereotactic injections of either AAV-NC or AAV-GfaABC1D-*Dmp1*shRNA into aged Cx43 cKO mice (Fig. 6A). Utilizing WFA, Aggrecan, and Golgi staining, we observed a significant reduction in the number of neurons enveloped by PNNs and in the dendritic spine count within the hippocampus of *Dmp1* knockdown mice

after anesthesia and surgery (Fig. 6D–G). These findings imply that the knockdown of *Dmp1* results in decreased PNNs and dendritic spine density in hippocampal neurons. Subsequent behavioral assessments demonstrated that the injection of AAV-GfaABC1D-sh*Dmp1* negated the cognitive enhancements conferred by astroglial Cx43 cKO following anesthesia and surgery (Fig. 6H–N). Collectively, these results indicate that *Dmp1* knockdown counteracts the neuroprotective effects of Cx43 cKO on PNNs formation and cognitive function amidst cognitive decline induced by anesthesia and surgery.

Fig. 5 Astroglial Cx43 cKO increases PNNs formation and the dendritic spine number in hippocampal neurons following anesthesia and surgery. **A** WFA-labeled PNNs in the hippocampus of 18-month-old *Gja1*$^{fl/fl}$ mice. **B** Representative confocal images of Aggrecan in the hippocampus of 18-month-old *Gja1*$^{fl/fl}$ mice. **C** Representative Golgi staining in the hippocampus of 18-month-old *Gja1*$^{fl/fl}$ mice. The data are presented as the means ± SDs ($n = 15$ for per group). **D** *Dmp1* mRNA expression in the hippocampus were analyzed via quantitative RT−PCR. *Gapdh* was used for normalization. n = 4 for per group. **E** Dmp1 protein expression in the hippocampus was analyzed via western blotting. β-Actin was used as a loading control. n = 4 for per group. The data were analyzed by Student's *t* test. Scale bar = 50 μm in A, B; 20 μm in E. *CTR* control, *AS* anesthesia and surgery

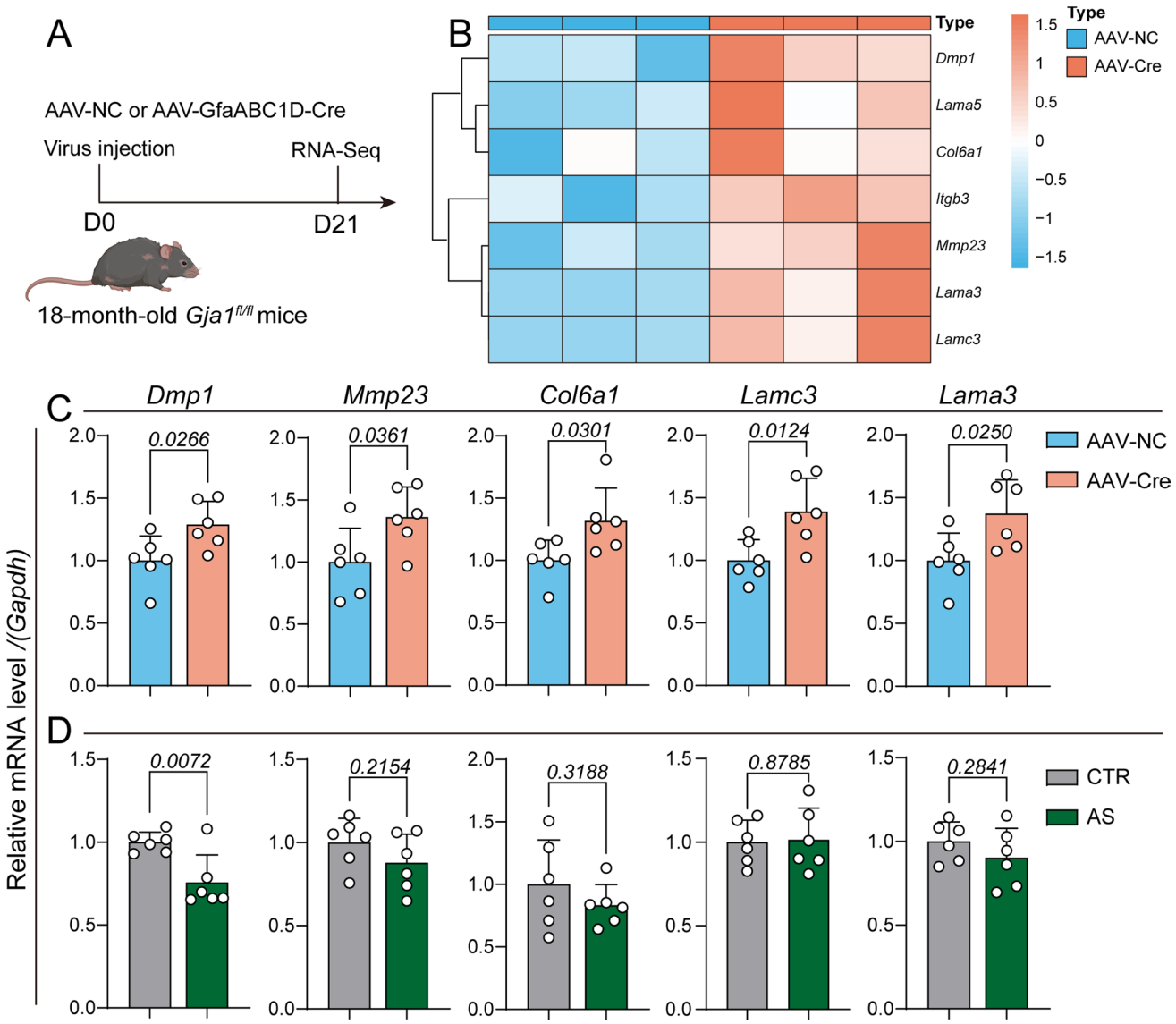

Fig. 4 Cytoplasmic Cx43 modulates the expression of the PNNs-related protein Dmp1 in astrocytes following anesthesia and surgery. **A** Schematic of virus injections into the bilateral hippocampus of aged *Gja1*$^{fl/fl}$ to conditionally knockout of astroglial Cx43 before RNA-seq. **B** Heatmaps of the upregulated genes $n = 3$ for per group. Validation of changes in the expression of selected genes in the hippocampus of astroglial Cx43 cKO mice (**C**) and 18-month-old C57BL/6 mice (**D**) with or without anesthesia and surgery by RT−PCR. $n = 6$ for per group. The data are presented as the means ± SDs and were analyzed by Student's *t* test. *CTR* control, *AS* anesthesia and surgery

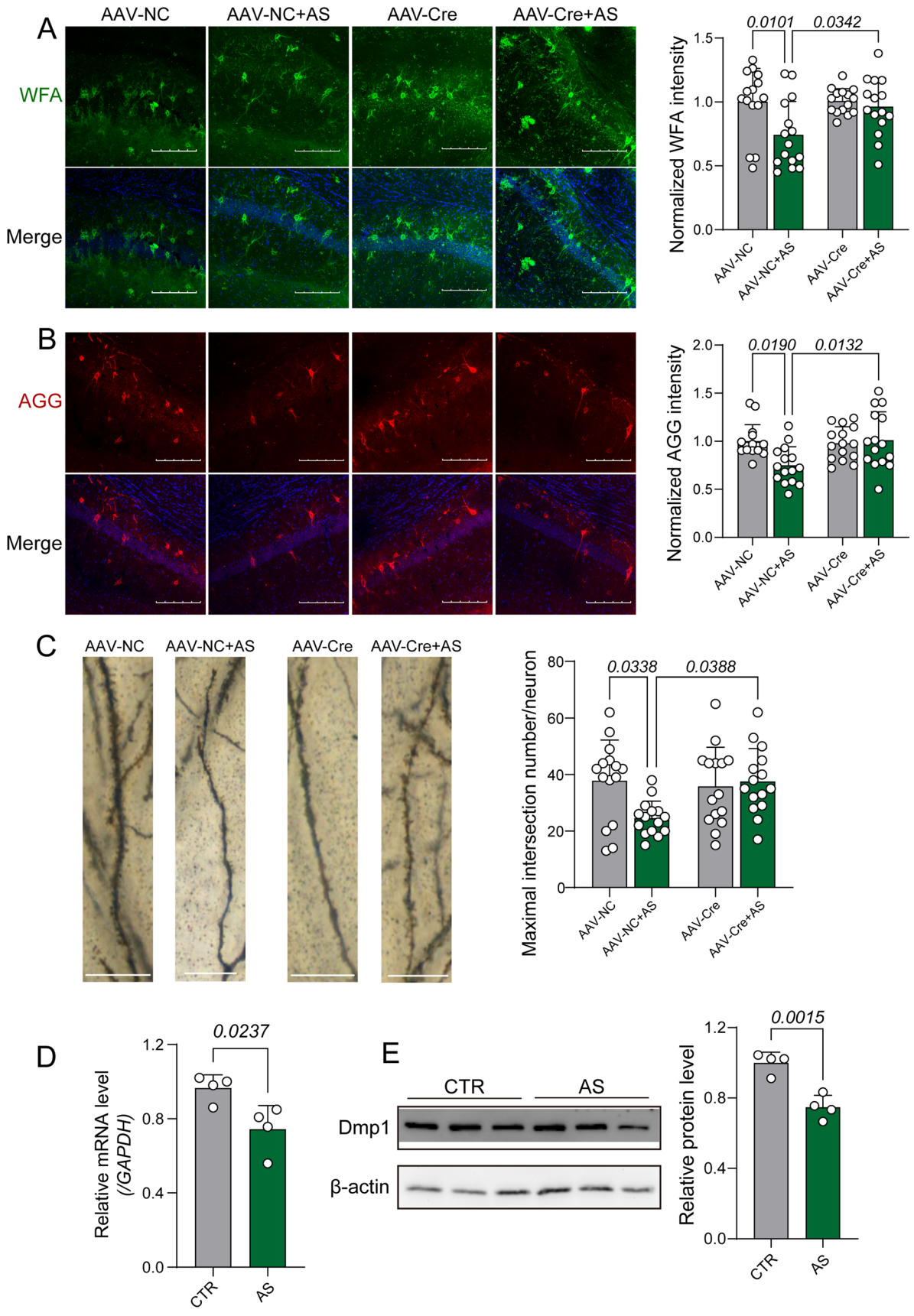
A
AAV-NC
AAV-NC+AS
AAV-Cre
AAV-Cre+AS
WFA
Merge
Normalized WFA intensity
0.0101
0.0342
B
AGG
Merge
Normalized AGG intensity
0.0190
0.0132
C
Maximal intersection number/neuron
0.0338
0.0388
D
Relative mRNA level (/GAPDH)
0.0237
CTR
AS
E
Dmp1
β-actin
Relative protein level
0.0015

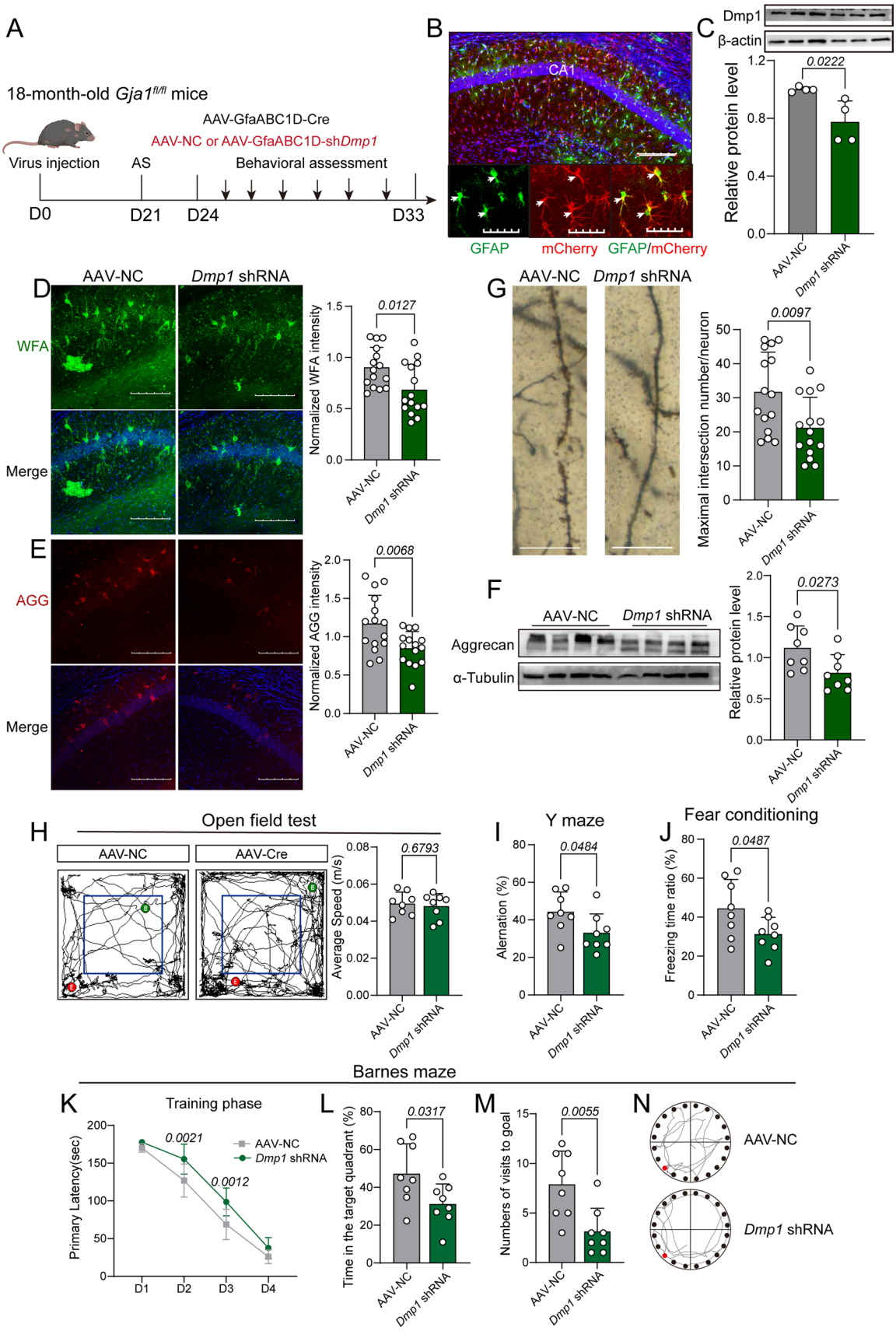
A
18-month-old Gja1fl/fl mice
AAV-GfaABC1D-Cre
AAV-NC or AAV-GfaABC1D-shDmp1
Virus injection
AS
Behavioral assessment
D0
D21
D24
D33
B
CA1
GFAP
mCherry
GFAP/mCherry
C
Dmp1
β-actin
0.0222
Relative protein level
AAV-NC
Dmp1 shRNA
D
AAV-NC
Dmp1 shRNA
WFA
Merge
0.0127
Normalized WFA intensity
E
AGG
Merge
0.0068
Normalized AGG intensity
F
AAV-NC
Dmp1 shRNA
Aggrecan
α-Tubulin
0.0273
Relative protein level
G
AAV-NC
Dmp1 shRNA
0.0097
Maximal intersection number/neuron
H
Open field test
AAV-NC
AAV-Cre
0.6793
Average Speed (m/s)
I
Y maze
0.0484
Alternation (%)
J
Fear conditioning
0.0487
Freezing time ratio (%)
Barnes maze
K
Training phase
0.0021
0.0012
AAV-NC
Dmp1 shRNA
Primary Latency(sec)
D1
D2
D3
D4
L
0.0317
Time in the target quadrant (%)
M
0.0055
Numbers of visits to goal
N
AAV-NC
Dmp1 shRNA

◂**Fig. 6** Astroglial Cx43 modulates PNNs formation and the dendritic spine number in the hippocampus through Dmp1 in aged mice. **A** Schematic of virus injections into the bilateral hippocampus of aged Cx43 cKO mice (*Gja1*$^{fl/fl}$ mice injected with AAV-GfaABC1D-Cre) (top). Schematic of the experimental timeline (bottom). **B** Representative confocal images of the mouse hippocampus showing AAV-infected astrocytes in the CA1 region. Blue: DAPI staining. Scale bars, 200 μm (top). Higher magnification images showing infected CA1 astrocytes. Scale bars, 50 μm (bottom). **C** Validation of the AAV-mediated blockade of *Dmp1* in the hippocampus via western blotting. β-Actin was used as a loading control. $n=4$ for per group. **D** WFA-labeled PNNs. **E** Representative confocal images of Aggrecan staining. **F** Aggrecan protein expression was assessed by western blotting. **G** Representative images of Golgi staining. $n=15$ for per group. **H** Representative trajectories and average speed in the OFT. **I** Percentage of spontaneous alternations in the Y-maze test. **J** Freezing time ratio in the CFT. **K–N** Training curve (4 consecutive days) (**K**), time spent in the target quadrant (**L**), number of visits to the goal (**M**), and representative trajectories of the animals (**N**) in the BM test. $n=8$ for per group in OFT, BM and CFT. The data are presented as the means ± SDs and were analyzed by one-way ANOVA, two-way ANOVA or Student's *t* test. Scale bar = 50 μm in **D**, **E** and 20 μm in **G**. AS, anesthesia and surgery

Sox2, a critical transcription factor in the regulation of *Dmp1*, was also investigated for its interaction with Cx43. We hypothesized that Cx43 might inhibit *Dmp1* transcription by binding to Sox2. Flow cytometry analysis indicated that the fluorescence intensity of cytoplasmic Cx43 exceeded that of membrane-bound Cx43 in aged mice after anesthesia and surgery (Supplemental Fig. 3A). Further assessment of the interaction between Cx43 and Sox2 in the hippocampal tissue and primary astrocytes revealed a significant crosstalk between the two proteins (Supplemental Fig. 3B and C). These findings suggested that Cx43 modulates *Dmp1* transcription by interacting with Sox2.

Discussion

In this study, we aimed to elucidate the specific regulatory mechanisms of Cx43 on PNNs and their pivotal role in the development of PND. Our findings indicate that anesthesia and surgery induce an upregulation of Cx43 expression, which in turn inhibits the formation of PNNs and dendritic spines in hippocampus by suppressing *Dmp1* transcription, leading to cognitive deficits in aged mice. We present several lines of evidence to substantiate this hypothesis. Firstly, qRT-PCR revealed an increase in total *Gja1* mRNA levels in the hippocampus of aged mice following anesthesia and surgery. Elevated astroglial *Gja1* levels were corroborated by in situ hybridization, and both total and soluble Cx43 levels were found to be significantly elevated. Notably, flow cytometry analysis indicated that the increase in astroglial Cx43 was primarily localized to the cytoplasm. Secondly, we employed two distinct strategies to modulate astroglial Cx43 expression prior to anesthesia and surgery in aged mice. Injections of AAV-GfaABC1D-shRNA*Gja1* into aged wild-type mice and AAV-GfaABC1D-Cre into aged into aged *Gja1*$^{fl/fl}$ mice resulted in improved learning and memory performance in the Y-maze, BM test, and CFT after anesthesia and surgery. Thirdly, astroglial Cx43 cKO was sufficient to increase the number of PNNs and dendritic spines in hippocampal neurons, which had been reduced by anesthesia and surgery. Fourthly, RNA sequencing data indicated that *Dmp1* expression was upregulated in the hippocampus of cKO mice. Aged cKO mice with astrocyte-specific *Dmp1* knockout exhibited a loss of PNNs and reduced dendritic spines, consistent with memory impairment. The transcription factor Sox2 is suggested to interact directly with Cx43 [34]. And Sox2, a key transcription factor, is known to regulate *Dmp1*. Our investigation into the interplay between Cx43 and Sox2 revealed that cytoplasmic Cx43 may actively control gene expression by interacting with transcription factors such as Sox2, thereby modulating PNNs in PND.

The role of Cx43 in PND has been highlighted, with its function as a gap junction (GJ) or hemichannel being of particular interest. Inhibition of Cx43 as a hemichannel has been shown to alleviate cognitive impairment in aged mice [35], while the enhancement of astroglial network function mediated by GJ Cx43 can ameliorate cognitive dysfunction induced by anesthesia [36]. Given this discrepancy, we investigated the differences in hippocampal Cx43 expression following different modeling conditions. Our results revealed that Cx43 expression was elevated following both anesthesia and surgery, irrespective of the surgical method used. In contrast, Cx43 expression also increased with anesthesia alone (Supplemental Fig. 4A). These findings suggest that Cx43 could serve as a pivotal biomarker for distinguishing cognitive dysfunction associated with dissociative anesthetics from that caused by the combination of anesthesia and surgery. Subsequently, we examined changes in hippocampal astrocyte Cx43 expression in young and aged mice, both before and after anesthesia and surgery. The results indicated that Cx43 expression in astrocytes was higher in 18-month-old mice compared to 6-week-old mice, and that anesthesia and surgery led to a further increase in Cx43 expression specifically in the aged mice. (Supplemental Fig. 4C and D). This observation could be instrumental in assessing the susceptibility of aged mice to PND. These seemingly contradictory findings may be attributed to differences in the age of the mice studied, as Cx43 expression decreases with aging. Moreover, our study has indicated that cytoplasmic Cx43 plays an active role in controlling gene expression via direct interactions with certain transcription factors, Sox2, to manipulate extracellular matrix in PND. This may provide a new insight in therapy of PND.

PNNs, prominent extracellular matrix structures in the CNS, are composed of a proteoglycan core protein

decorated with chondroitin sulfate chains. The role of the extracellular matrix in memory-related plasticity is increasingly recognized [11, 37]. Matrix metallopeptidase 9 (MMP9), which degrades extracellular matrix structures and contributes to blood–brain barrier opening and neuroinflammation, is upregulated by surgery [12, 14]. Dmp1, crucial for extracellular matrix formation [38, 39], was identified as a key player in the response to anesthesia and surgery, with its expression being specifically altered under these conditions. Our RNA-seq results revealed an increase in various PNNs-related genes in the hippocampus of Cx43 cKO mice, with *Dmp1* being a central regulator.

In conclusion, this study provides novel mechanistic insights into the pathogenesis of PND and identifies potential targets for therapeutic intervention. It highlights the role of Cx43 in modulating PNNs and its significant contribution to cognitive function following anesthesia and surgery.

Supplementary Information The online version contains supplementary material available at https://doi.org/10.1007/s00018-024-05530-7.

Acknowledgements Not applicable.

Author contributions Q.Z., Y.X.Z., P.L.C., Q.Q.W., H.X.W., X.W.H., X.Y.L., Z.X.L., and H.H.W. conducted the in vitro and in vivo experiments. Behavioral tests were executed by Q.Z., Y.X.Z., and P.L.C., who also undertook the data analysis. L.Z.X., L.T., H.H.W., P.L.C., and X.W.H. offered valuable guidance throughout the study. Manuscript preparation was handled by Q.Z., Y.X.Z., and P.L.C., with contributions from L.T. The overall research was conceptualized and overseen by L.Z.X.

Funding Financial support for this research was provided by the National Natural Science Foundation of China, with grant numbers 82130121, 82293640, 82201344, 82101256, and 82301370. Additionally, the work was funded by the Scientific and Technological Innovation 2030-Major Project of Brain Science and Brain-Like Intelligence Technology, with grant number 2021ZD0202804. Further support came from the Second Round of the Three-Year Action Plan for Strengthening and Promoting Traditional Chinese Medicine of Hongkou District, with grant number HKGYQYXM-2022-06, and the Scientific Research Funds of Shanghai Fourth People's Hospital, with grant numbers sykyqd08701, KY-XKZT-2022-1008, and SY-XKZT-2023-1005.

Data availability The research data generated during this study are accessible upon a reasonable request made to the corresponding author.

Declarations

Conflict of interest The authors declare that they have no financial or nonfinancial interests that could be perceived as relevant to the research reported.

Ethical approval The study's experimental procedures were granted approval by the Animal Care and Use Committee at Tongji University, located in Shanghai, China, under the specific approval number TJBH07922101.

Consent for publication Not applicable.

References

1. Turan A, Duncan A, Leung S, Karimi N, Fang J, Mao G, Hargrave J, Gillinov M, Trombetta C, Ayad S et al (2020) Dexmedetomidine for reduction of atrial fibrillation and delirium after cardiac surgery (DECADE): a randomised placebo-controlled trial. Lancet 396(10245):177–185
2. Deiner S, Luo X, Lin H-M, Sessler DI, Saager L, Sieber FE, Lee HB, Sano M, Jankowski C, Bergese SD et al (2017) Intraoperative infusion of dexmedetomidine for prevention of postoperative delirium and cognitive dysfunction in elderly patients undergoing major elective noncardiac surgery: a randomized clinical trial. JAMA Surg 152(8):e171505
3. Humeidan ML (2021) Reyes J-PC, Mavarez-Martinez A, Roeth C, Nguyen CM, Sheridan E, Zuleta-Alarcon A, Otey A, Abdel-Rasoul M, Bergese SD: Effect of cognitive prehabilitation on the incidence of postoperative delirium among older adults undergoing major noncardiac surgery: the Neurobics Randomized Clinical Trial. JAMA Surg 156(2):148–156
4. Subramaniam B, Shankar P, Shaefi S, Mueller A, O'Gara B, Banner-Goodspeed V, Gallagher J, Gasangwa D, Patxot M, Packiasabapathy S et al (2019) Effect of intravenous acetaminophen vs placebo combined with propofol or dexmedetomidine on postoperative delirium among older patients following cardiac surgery: The DEXACET randomized clinical trial. JAMA 321(7):686–696
5. Neuman MD, Feng R, Carson JL, Gaskins LJ, Dillane D, Sessler DI, Sieber F, Magaziner J, Marcantonio ER, Mehta S et al (2021) Spinal anesthesia or general anesthesia for hip surgery in older adults. N Engl J Med 385(22):2025–2035
6. Li T, Li J, Yuan L, Wu J, Jiang C, Daniels J, Mehta RL, Wang M, Yeung J, Jackson T et al (2022) Effect of regional vs general anesthesia on incidence of postoperative delirium in older patients undergoing hip fracture surgery: The RAGA randomized trial. JAMA 327(1):50–58
7. Su X, Meng Z-T, Wu X-H, Cui F, Li H-L, Wang D-X, Zhu X, Zhu S-N, Maze M, Ma D (2016) Dexmedetomidine for prevention of delirium in elderly patients after non-cardiac surgery: a randomised, double-blind, placebo-controlled trial. Lancet 388(10054):1893–1902
8. Mortensen CB, Andersen-Ranberg NC, Poulsen LM, Granholm A, Rasmussen BS, Kjær MBN, Lange T, Ebdrup BH, Collet MO, Andreasen AS et al (2024) Long-term outcomes with haloperidol versus placebo in acutely admitted adult ICU patients with delirium. Intensive Care Med 50(1):103–113
9. Villalobos D, Reese M, Wright MC, Wong M, Syed A, Park J, Hall A, Browndyke JN, Martucci KT, Devinney MJ et al (2023) Perioperative changes in neurocognitive and Alzheimer's

disease-related cerebrospinal fluid biomarkers in older patients randomised to isoflurane or propofol for anaesthetic maintenance. Br J Anaesth 131(2):328–337
10. Fawcett JW, Fyhn M, Jendelova P, Kwok JCF, Ruzicka J, Sorg BA (2022) The extracellular matrix and perineuronal nets in memory. Mol Psychiatry 27(8):3192–3203
11. Feng H, Zhang Z, Lyu W, Kong X, Li J, Zhou H, Wei P (2023) The effects of appropriate perioperative exercise on perioperative neurocognitive disorders: a narrative review. Mol Neurobiol 61:4663–4676
12. Ni P, Dong H, Wang Y, Zhou Q, Xu M, Qian Y, Sun J (2018) IL-17A contributes to perioperative neurocognitive disorders through blood-brain barrier disruption in aged mice. J Neuroinflammation 15(1):332
13. Li Y, Chen L, Li Z, Song Y, Yuan Y, Liu T, Hong J, Wang Q, Chang H, Kuang Z et al (2021) Potential serum biomarkers for postoperative neurocognitive disorders based on proteomic analysis of cognitive-related brain regions. Front Aging Neurosci 13:741263
14. Zhu B, Cao A, Chen C, Zhou W, Luo W, Gui Y, Wang Q, Xu Z, Wang J (2024) MMP-9 inhibition alleviates postoperative cognitive dysfunction by improving glymphatic function via regulating AQP4 polarity. Int Immunopharmacol 126:111215
15. Tansley S, Gu N, Guzmán AU, Cai W, Wong C, Lister KC, Muñoz-Pino E, Yousefpour N, Roome RB, Heal J et al (2022) Microglia-mediated degradation of perineuronal nets promotes pain. Science 377(6601):80–86
16. Fawcett JW, Oohashi T, Pizzorusso T (2019) The roles of perineuronal nets and the perinodal extracellular matrix in neuronal function. Nat Rev Neurosci 20(8):451–465
17. Brückner G, Szeöke S, Pavlica S, Grosche J, Kacza J (2006) Axon initial segment ensheathed by extracellular matrix in perineuronal nets. Neuroscience 138(2):365–375
18. Gogolla N, Caroni P, Lüthi A, Herry C (2009) Perineuronal nets protect fear memories from erasure. Science 325(5945):1258–1261
19. Banerjee SB, Gutzeit VA, Baman J, Aoued HS, Doshi NK, Liu RC, Ressler KJ (2017) Perineuronal nets in the adult sensory cortex are necessary for fear learning. Neuron 95(1):169
20. Eggers SDZ, Horn AKE, Roeber S, Härtig W, Nair G, Reich DS, Leigh RJ (2015) Saccadic palsy following cardiac surgery: possible role of perineuronal nets. PLoS ONE 10(7):e0132075
21. Sorgen PL, Trease AJ, Spagnol G, Delmar M, Nielsen MS (2018) Protein–protein interactions with connexin 43: regulation and function. Int J Mol Sci 19(5):1428
22. Winterhager E, Kidder GM (2015) Gap junction connexins in female reproductive organs: implications for women's reproductive health. Hum Reprod Update 21(3):340–352
23. Jiang H, Zhang Y, Wang Z-Z, Chen N-H (2023) Connexin 43: an interface connecting neuroinflammation to depression. Molecules 28(4):1820
24. Epifantseva I, Shaw RM (2018) Intracellular trafficking pathways of Cx43 gap junction channels. Biochim Biophys Acta Biomembr 1860(1):40–47
25. Martins-Marques T, Ribeiro-Rodrigues T, Batista-Almeida D, Aasen T, Kwak BR, Girao H (2019) Biological functions of connexin43 beyond intercellular communication. Trends Cell Biol 29(10):835–847
26. Mei X, Ezan P, Giaume C, Koulakoff A (2010) Astroglial connexin immunoreactivity is specifically altered at β-amyloid plaques in β-amyloid precursor protein/presenilin1 mice. Neuroscience 171(1):92–105
27. Ren R, Zhang L, Wang M (2018) Specific deletion connexin43 in astrocyte ameliorates cognitive dysfunction in APP/PS1 mice. Life Sci 208:175–191
28. Cogliati B, Vinken M, Silva TC, Araújo CMM, Aloia TPA, Chaible LM, Mori CMC, Dagli MLZ (2015) Connexin 43 deficiency accelerates skin wound healing and extracellular matrix remodeling in mice. J Dermatol Sci 79(1):50–56
29. Zhang Q, Cong P, Tian L, Wu T, Huang X, Zhang Y, Wu H, Liang H, Xiong L (2024) Exercise attenuates the perioperative neurocognitive disorder induced by hyperhomocysteinemia in mice. Brain Res Bull 209:110913
30. Xu F, Cong P, Zhang B, Dong H, Zuo W, Wu T, Tian L, Xiong L (2023) A decrease in NR2B expression mediated by DNA hypermethylation induces perioperative neurocognitive disorder in aged mice. CNS Neurosci Ther 29(5):1229–1242
31. Wu T, Li M, Tian L, Cong P, Huang X, Wu H, Zhang Q, Zhang H, Xiong L (2023) A modified mouse model of perioperative neurocognitive disorders exacerbated by sleep fragmentation. Exp Anim 72(1):55–67
32. Shi W, Wei X, Wang X, Du S, Liu W, Song J, Wang Y (2019) Perineuronal nets protect long-term memory by limiting activity-dependent inhibition from parvalbumin interneurons. Proc Natl Acad Sci U S A 116(52):27063–27073
33. Jing B, Zhang C, Liu X, Zhou L, Liu J, Yao Y, Yu J, Weng Y, Pan M, Liu J et al (2018) Glycosylation of dentin matrix protein 1 is a novel key element for astrocyte maturation and BBB integrity. Protein Cell 9(3):298–309
34. Mahlokozera T, Patel B, Chen H, Desouza P, Qu X, Mao DD, Hafez D, Yang W, Taiwo R, Paturu M et al (2021) Competitive binding of E3 ligases TRIM26 and WWP2 controls SOX2 in glioblastoma. Nat Commun 12(1):6321
35. Ju H, Wang Y, Shi Q, Zhou Y, Ma R, Wu P, Fang H (2019) Inhibition of connexin 43 hemichannels improves postoperative cognitive function in aged mice. Am J Transl Res 11(4):2280–2287
36. Dong R, Han Y, Jiang L, Liu S, Zhang F, Peng L, Wang Z, Ma Z, Xia T, Gu X (2022) Connexin 43 gap junction-mediated astrocytic network reconstruction attenuates isoflurane-induced cognitive dysfunction in mice. J Neuroinflammation 19(1):64
37. Rowlands D, Lensjø KK, Dinh T, Yang S, Andrews MR, Hafting T, Fyhn M, Fawcett JW, Dick G (2018) Aggrecan directs extracellular matrix-mediated neuronal plasticity. J Neurosci 38(47):10102–10113
38. Liu S, Zhou J, Tang W, Menard R, Feng JQ, Quarles LD (2008) Pathogenic role of Fgf23 in Dmp1-null mice. Am J Physiol Endocrinol Metab 295(2):E254–E261
39. Basu-Roy U, Ambrosetti D, Favaro R, Nicolis SK, Mansukhani A, Basilico C (2010) The transcription factor Sox2 is required for osteoblast self-renewal. Cell Death Differ 17(8):1345–1353